All-polarization-maintaining figure-eight Er-fiber ultrafast laser with a bidirectional output coupler in the loss-imbalanced nonlinear optical loop mirror

Junkai Shi (石俊凯)[1], Yao Li (黎 尧)[1], Shuyuan Gao (高书苑)[1], Yingling Pan (潘映伶)[1], Guoming Wang (王国名)[1], Rongyi Ji (纪荣祎)[1], and Weihu Zhou (周维虎)[1,2,*]

[1]*Laboratory of Laser Measurement Technology, Academy of Opto-Electronics, Chinese Academy of Sciences, Beijing 100094, China*

[2]*University of Chinese Academy of Sciences, Beijing 100049, China*

**Corresponding author: zhouweihu@aoe.ac.cn*

Received September 3, 2018; accepted November 1, 2018; posted online November 27, 2018

In this Letter, we report on a novel architecture for a self-starting mode-locked figure-eight erbium-doped fiber laser using a loss-imbalanced nonlinear optical loop mirror (NOLM) with a bidirectional output coupler. An all-polarization-maintaining structure is adopted. A 2×2 optical coupler with a splitting ratio of 50:50 is used at the junction to form an NOLM. Another coupler with a splitting ratio of 10:90 is introduced at one end of the fiber loop. The 10:90 coupler plays two roles: power attenuator and bidirectional output coupler. This architecture can achieve both large modulation depth and good self-starting ability simultaneously. With this architecture, the self-starting mode-locking operation is achieved easily with pump power above the threshold. The clockwise and counter-clockwise mode-locked output powers are 10.1 and 10.3 mW, respectively, with the repetition rate of 3.63 MHz. The spectral bandwidths of the clockwise and counter-clockwise mode-locked output pulses are 7.4 and 2.9 nm, and the corresponding pulse widths of the direct outputs are 530.6 fs and 1.55 ps, respectively.

OCIS codes: 140.3510, 140.4050, 140.7090.
doi: 10.3788/COL201816.121404.

Over the last decades, the mode-locked fiber laser has attracted considerable attention because of its widespread applications in spectroscopy, optical communication, microscopy, and precision metrology[1–3]. Compared with actively mode-locked fiber lasers, passively mode-locked fiber lasers are preferred due to their intriguing advantages, such as ultrashort pulses, compactness, and low cost. In order to achieve passive mode locking, both material-based saturable absorbers (SAs) and artificial SAs have been extensively studied.

Material-based SAs, such as a semiconductor SA mirror[4,5], graphene[6,7], carbon nanotubes[8,9], and topological insulators[10,11], are frequently used in passively mode-locked fiber lasers. These SAs offer easy self-starting and environmentally stable mode locking with a simple cavity design. However, such intrinsic SAs in fiber lasers suffer from the relatively low damage threshold, potential degradation over time, long recovery time, and consequent large timing jitter, which limits their applications mainly to laboratory use.

The artificial SAs include nonlinear polarization rotation (NPR)[12,13], nonlinear optical loop mirror (NOLM)[14,15], nonlinear amplifying loop mirror (NALM)[16,17], and Mamyshev oscillator[18,19]. Compared with the material-based SAs, artificial SAs have shown the advantages of considerably higher damage threshold, extremely shorter response time, and therefore, potentially lower intrinsic noise. The NPR mechanism is a prominent example of artificial SAs in fiber lasers. In the NPR mode-locked fiber laser, the key is precise control of the intracavity light polarization state, resulting in high sensitivity to the environmental perturbations and mechanical vibrations. The polarization-maintaining (PM) fiber cavity can markedly improve the environmental stability, but the traditional NPR mode-locked fiber laser is incompatible with PM fiber due to its intrinsic mechanism. Many efforts have been made to realize an NPR mode-locked PM fiber laser[20–22], which is extremely helpful in overcoming stability problems. The Mamyshev oscillator based on two Mamyshev regenerators has been reported most recently, and multi-megawatt peak power has been achieved[18,19]. But the Mamyshev oscillator lacks the self-starting ability, and the free space part of the cavity decreases the environmental stability.

In recent years, NOLM and NALM have attracted more interest. NOLM and NALM are promising candidates for a mode locker in fiber lasers, because they have the advantages of short response time, high damage threshold, and the possibility of all-PM fiber implementation. NOLM and NALM were first mentioned in 1988[23] and 1990[24], respectively. Since then, NOLM- and NALM-based mode-locked fiber lasers have been extensively studied[14–17,25–27]. With an asymmetric beam splitter used at the junction, the intensity dependence of the NOLM is caused by a differential phase shift between the two counter-propagating pulses. A small beam splitting ratio results in a small differential laser intensity, and the nonlinear phase shift accumulates slowly in pace with the increase of laser intensity or fiber loop length. The large beam splitting ratio is helpful in

accelerating accumulation of the nonlinear phase shift, but it also reduces the modulation depth. So, it is difficult to achieve the self-starting operation in fiber lasers based on NOLM and NALM. Both the two-gain-segment design[16,28,29] and nonreciprocal phase shifter[30–33] can improve the self-starting ability and also complicate the cavity structure.

In this article, an all-PM figure-eight mode-locked erbium-doped fiber (EDF) laser based on loss-imbalanced NOLM is demonstrated. A 2×2 optical coupler (OC) with a splitting ratio of 50∶50 is used at the junction to achieve maximum modulation depth. An asymmetric coupler with a splitting ratio of 10∶90 is introduced at one end of the fiber loop to generate nonlinear phase shift and extract 90% of the average power of the counter-propagating pulses as laser outputs. With the pump power above the threshold, the self-starting single pulse mode-locking operation is achieved easily. Finally, the clockwise (CW) and counter-clockwise (CCW) output powers are 10.1 and 10.3 mW, respectively, with pulse energy of 2.78 and 2.84 nJ. The direct output pulse widths are 530.6 fs and 1.55 ps, respectively.

A bidirectional power attenuator is introduced in the NOLM to construct a loss-imbalanced NOLM, as shown in Ref. [34]. The power splitting ratio of NOLM is α: $(1-\alpha)$, where $0 \le \alpha \le 0.5$. The power attenuator is located at one end of the fiber loop, and the transmissivity for both directions is β $(0 \le \beta \le 1)$. With an input field E_{in}, the normalized transmissivity T_0 and reflectivity R_0 of the NOLM are given by[23,34]

$$T_0 = 1 - 2\alpha(1-\alpha)\left\{1 + \cos\left[(\alpha - \beta + \alpha\beta)\frac{2\pi n_2}{\lambda}|E_{\mathrm{in}}|^2 L\right]\right\}, \tag{1}$$

$$R_0 = 2\alpha(1-\alpha)\left\{1 + \cos\left[(\alpha - \beta + \alpha\beta)\frac{2\pi n_2}{\lambda}|E_{\mathrm{in}}|^2 L\right]\right\}, \tag{2}$$

where n_2 is the nonlinear coefficient, λ is the operating wavelength, and L is the length of the loop fiber.

In the popular figure-eight configuration, the NOLM is operated in transmission. Figure 1 shows the normalized transmissivity and the slope of normalized transmissivity as a function of $|E_{\mathrm{in}}|^2 L$ with different beam splitting ratios. $|E_{\mathrm{in}}|^2 L$ is calculated by Eq. (1) and its derivative with $n_2 = 2 \times 10^{-20}$ m^2/W and $\lambda = 1550$ nm. The self-starting ability is related to the slope of the transmissivity curve, intracavity laser intensity, and length of the fiber loop. In the case of fixed loop length, the large slope of transmissivity corresponding to low laser intensity can enhance the self-starting ability[30,31]. With a splitting ratio of 45∶55 and no power attenuator, the transmissivity shown with a red dash curve exhibits large modulation depth, but the maximum slope of the transmissivity is relatively small, even with large $|E_{\mathrm{in}}|^2 L$, which results in a poor self-starting performance. When the splitting ratio is changed to 10∶90, the transmissivity shown with a blue short dash curve increases much faster, and the maximum slope is much larger with smaller $|E_{\mathrm{in}}|^2 L$. But, the modulation depth reduces considerably, which is detrimental to the single pulse mode-locking operation. In order to solve this problem, a power attenuator with a transmissivity of 10% is introduced in the symmetric fiber loop to form a loss-imbalanced NOLM. As shown with black solid curve in Fig. 1, the modulation depth remains at the maximum value, and the maximum slope value is larger than that of the 10∶90 splitting ratio with similar $|E_{\mathrm{in}}|^2 L$, which means better self-starting ability. Accordingly, the loss-imbalanced NOLM can achieve both large modulation depth and good self-starting ability simultaneously.

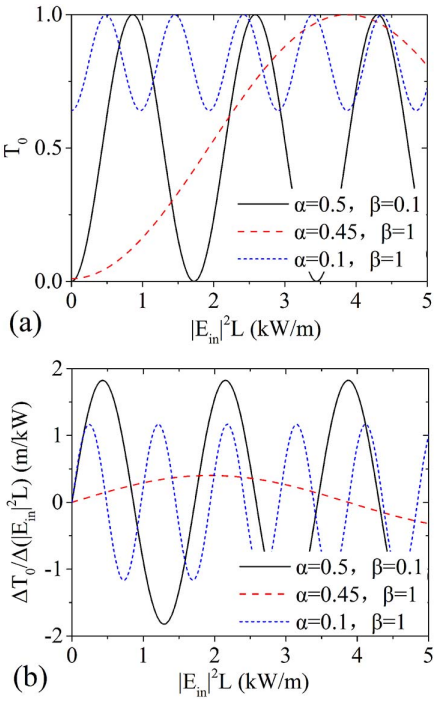

Fig. 1. (a) Normalized transmissivity and (b) the slope of normalized transmissivity as a function of $|E_{\mathrm{in}}|^2 L$ under the conditions of the symmetric coupler with a power attenuator ($\alpha = 0.5$, $\beta = 0.1$, black solid curve), small splitting ratio ($\alpha = 0.45$, $\beta = 1$, red dash curve), and large splitting ratio ($\alpha = 0.1$, $\beta = 1$, blue short dash curve) without a power attenuator.

Based on the loss-imbalanced NOLM described above, an all-PM figure-eight EDF ultrafast laser is constructed, as shown in Fig. 2. A 2×2 3 dB PM fiber coupler (OC_1) is used at the junction to achieve maximum modulation depth. The unidirectional ring cavity is formed with a piece of 2 m PM EDF (PM-ESF-7/125, Nufern). The PM EDF has a mode field diameter of 8.8 μm, a group velocity dispersion of -0.02 ps^2/m, and a core absorption of 55 dB/m at 1530 nm. A 976 nm laser diode (LD) delivering a maximum output power of 800 mW is used as a pump source. The pump laser is coupled into the cavity through a standard PM 976/1550 nm wavelength division multiplexer (WDM). A polarization-dependent optical isolator (OI) is used to ensure the unidirectional

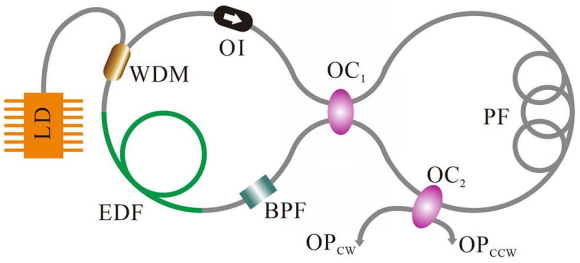

Fig. 2. Schematic of the experimental setup: LD, laser diode; WDM, wavelength division multiplexer; OC, optical coupler; EDF, Er-doped fiber; BPF, bandpass filter; PF, passive fiber; OI, optical isolator; OP, output.

operation. A 2 nm bandpass filter (BPF) centered at 1550 nm acts to block longer wavelengths (Raman self-frequency shift) and decrease the temporal duration of the pulse in the cavity in order for the pulse to rapidly evolve back over the next roundtrip. For the loss-imbalanced NOLM described above, the maximum transmissivity is only β. To avoid energy loss, a 10:90 coupler (OC_2) is used as a power attenuator to generate nonlinear phase shift and extract 90% of the average power of the laser pulses propagating CW and CCW as laser outputs (OP_{CW}, OP_{CCW}). A piece of 50 m PM passive fiber (PF) is utilized to generate enough nonlinear phase shift for starting mode locking. The group velocity dispersion of the PF is -0.022 ps^2/m, and the net cavity dispersion is estimated to -1.24 ps^2. An optical spectrum analyzer (YOKOGAWA, AQ6370D), a radio-frequency analyzer (KEYSIGHT, N9010 A), and a digital storage oscilloscope (KEYSIGHT, DSO9254 A) together with a 1 GHz photo detector are employed to monitor the optical spectrum, the radio-frequency spectrum, and the output pulse train, respectively. Additionally, the pulse profile is measured by a commercial autocorrelator (APE PulseCheck).

In this experiment, the self-starting single pulse mode locking is easily achieved when the pump power exceeds 510 mW. The characteristics of mode-locked outputs are shown in Figs. 3 and 4. As shown in Fig. 3, the CW and CCW output powers increase linearly as the pump power rises. The fiber laser can sustain the mode-locking state when the pump power is decreased to 456 mW because of the pump hysteresis phenomenon[35].

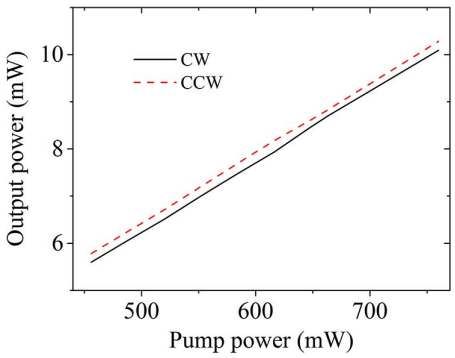

Fig. 3. Output power as a function of pump power.

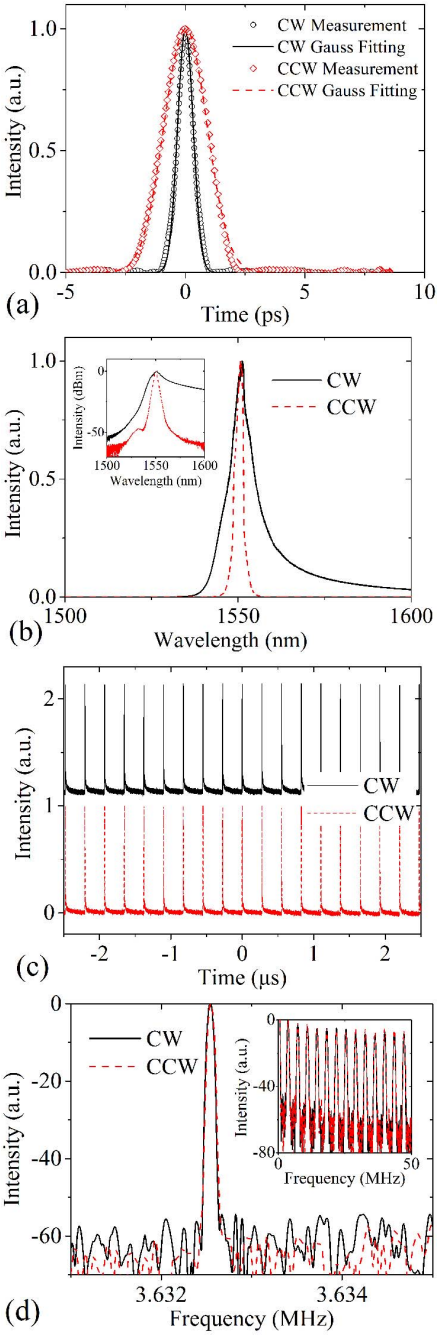

Fig. 4. Mode-locked outputs of the figure-eight oscillator at the pump power of 760 mW. Experimentally observed (a) autocorrelation traces, (b) spectra in the linear scale (inset: spectra in log scale), (c) pulse trains, and (d) radio-frequency spectra (inset: radio-frequency spectra in a wider range) of the CW and CCW output pulses.

The CW and CCW output powers are 10.1 and 10.3 mW with the available maximum pump power of 760 mW, and the total slope efficiency is about 3%. The low slope efficiency is mainly caused by large cavity loss, resulting from a large coupling output coefficient and narrowband filter. The laser works in the single pulse regime with pump power from 456 to 760 mW, which benefits from the very low intracavity pulse energy and large

modulation depth. The intracavity nonlinear effect is weak because of low intracavity pulse energy, which is helpful in avoiding wave breaking. The large modulation depth helps to eliminate the weaker intracavity pulses. The low intracavity pulse energy and large modulation depth ensure single pulse operation. The CW output power is slightly lower than the CCW output power, largely due to the transmission loss and splice loss of the fiber loop.

Figures 4(a) and 4(b) present the autocorrelation traces and optical spectra of the CW and CCW output pulses. The inset of Fig. 4(b) shows the optical spectra in log scale. The full widths at half-maximum (FWHMs) of 750.3 fs and 2.19 ps are obtained by fitting the autocorrelation traces with the Gaussian function. The pulse widths are estimated to be 530.6 fs and 1.55 ps. Compared with previous reports on the figure-eight mode-locked EDF laser with a repetition rate less than 10 MHz, the pulse widths are much shorter, which is mainly attributed to the soliton effect in negative dispersion fibers and narrow band filter. The central wavelengths defined by the central point of the 3 dB spectral bandwidth are 1551.1 and 1550.2 nm, respectively. The FWHMs of the spectra are 7.4 and 2.9 nm, and the corresponding time-bandwidth products are 0.49 and 0.56. Furthermore, the CW spectrum displays the obvious asymmetry. The intensity of the red region decreases much slower than the blue region. The CCW output pulse can be assumed as the NOLM input pulse, because it exits shortly after entering the fiber loop. The CW output pulse can be assumed as the NOLM output pulse. When the input pulse propagates in the negative dispersion fiber, it will undergo self-compression in the time domain and spectral broadening due to self-phase modulation[36]. With a symmetrical pulse profile, the spectral broadening is symmetric. The long-wave wing of the spectrum can be attributed to the nonlinear Raman conversion of the original pulse[37].

The pulse trains recorded by the oscilloscope are shown in Fig. 4(c). The period of the pulse trains is about 275.3 ns, which matches with the cavity roundtrip time and verifies the mode-locked state. The radio-frequency spectra around the fundamental repetition rate are measured with a resolution of 5 Hz and shown in Fig. 4(d), and the inset shows a wider range distribution of the radio-frequency spectra. The signal-to-noise ratios of 55 and 60 dB indicate excellent stability of the soliton mode locking. The fundamental repetition rates are 3.63 MHz, which agree well with the period of the pulse trains. The corresponding pulse energies of the CW and CCW outputs are 2.78 and 2.84 nJ, respectively.

As a contrast, a conventional figure-eight fiber laser based on NOLM with a small splitting ratio is also constructed. OC_1 is replaced by an OC with a splitting ratio of 45∶55. OC_2 is moved to the position between the BPF and OC_1 and works in the unidirectional mode. With the available maximum pump power, the mode-locking operation cannot be achieved, which approves the benefit of the proposed architecture.

In conclusion, we have experimentally investigated a self-starting all-PM figure-eight EDF mode-locked laser based on the loss-imbalanced NOLM. A bidirectional output coupler with an output coefficient of 90% is introduced at one end of the symmetric fiber loop to achieve large modulation depth and improve self-starting performance. This setup provides two pulse trains with different temporal and spectral characteristics, which can be useful for applications. The self-starting mode-locking operation is achieved easily, and this laser is immune to the environmental perturbations and mechanical vibrations. This method can also improve the self-starting ability of NALM-based or phase biased NOLM-based mode-locked fiber lasers.

This work was supported by the Key Project of Bureau of International Cooperation, Chinese Academy of Sciences (No. 181811KYSB20160029) and the Key Research Project of Bureau of Frontier Sciences and Education, Chinese Academy of Sciences (No. QYZDY-SSW-JSC008).

References

1. J. Shi and W. Zhou, Chin. Opt. Lett. **16**, 031404 (2018).
2. X. Zhao, Z. Zheng, L. Liu, Y. Liu, Y. Jiang, X. Yang, and J. Zhu, Opt. Express **19**, 1168 (2011).
3. S. Huang, Y. Wang, P. Yan, J. Zhao, H. Li, and R. Lin, Opt. Express **22**, 11417 (2015).
4. F. Lian, Z. Fan, Z. Bai, X. Li, and Q. Wang, Photon. Res. **3**, 129 (2015).
5. I. Armas-Rivera, C. Cuadrado-Laborde, A. Carrascosa, E. Kuzin, G. Beltran-Perez, A. Diez, and M. Andres, Opt. Express **24**, 9966 (2016).
6. J. Boguslawski, J. Sotor, G. Sobon, R. Kozinski, K. Librant, M. Aksienionek, L. Lipinska, and K. Abramski, Photon. Res. **3**, 119 (2015).
7. G. Zhu, X. Zhu, F. Wang, S. Xu, Y. Li, X. Guo, K. Balakrishnan, R. Norwood, and N. Peyghambarian, IEEE Photon. Technol. Lett. **28**, 7 (2016).
8. L. Hou, H. Guo, Y. Wang, J. Sun, Q. Lin, Y. Bai, and J. Bai, Opt. Express **26**, 9063 (2018).
9. X. Han, Appl. Opt. **57**, 807 (2018).
10. L. Li, Y. Su, Y. Wang, X. Wang, Y. Wang, X. Li, D. Mao, and J. Si, IEEE J. Sel. Top. Quantum Electron. **23**, 1100306 (2017).
11. J. Wang, Z. Jiang, H. Chen, J. Li, J. Yin, J. Wang, T. He, P. Yan, and S. Ruan, Photon. Res. **6**, 535 (2018).
12. J. Zhang, Z. Kong, Y. Liu, A. Wang, and Z. Zhang, Photon. Res. **4**, 27 (2016).
13. Q. Kuang, L. Zhan, Z. Gu, and Z. Wang, J. Lightwave Technol. **33**, 391 (2015).
14. J. Szczepanek, T. Kardas, M. Michalska, C. Radzewicz, and Y. Stepanenko, Opt. Lett. **40**, 3500 (2015).
15. S. Aleshkina, M. Bubnov, A. Senatorov, D. Lipatov, and M. Likhachev, Laser Phys. Lett. **13**, 035104 (2016).
16. J. Sun, Y. Zhou, Y. Dai, J. Li, F. Yin, J. Dai, and K. Xu, Appl. Opt. **57**, 1492 (2018).
17. K. Krzempek and K. Abramski, Opt. Express **24**, 22379 (2016).
18. Z. Liu, Z. Ziegler, L. Wright, and F. Wise, Optica **4**, 649 (2017).
19. P. Sidorenko, W. Fu, L. Wright, M. Olivier, and F. Wise, Opt. Lett. **43**, 2672 (2018).

20. W. Zhang, Y. Liu, C. Wang, Z. Zhu, D. Luo, C. Gu, and W. Li, Opt. Express **26**, 7934 (2018).
21. J. Szczepanek, T. Kardas, C. Radzewicz, and Y. Stepanenko, Opt. Express **26**, 13590 (2018).
22. J. Zhou, W. Pan, X. Gu, L. Zhang, and Y. Feng, Opt. Express **26**, 4166 (2018).
23. N. Doran and D. Wood, Opt. Lett. **13**, 56 (1988).
24. M. Fermann, F. Haberl, M. Hofer, and H. Hochreiter, Opt. Lett. **15**, 752 (1990).
25. S. Wu, J. Strait, and R. Fork, Opt. Lett. **18**, 1444 (1993).
26. J. Haus, G. Shaulov, E. Kuzin, and J. Sanchez-Mondragon, Opt. Lett. **24**, 376 (1999).
27. O. Pottiez, E. Kuzin, B. Ibarra-Escamilla, J. Camas-Anzueto, and F. Gutierrez-Zainos, Opt. Express **12**, 3878 (2004).
28. Y. Liu, W. Li, X. Shen, C. Wang, Z. Yang, and H. Zeng, IEEE Photon. Technol. Lett. **26**, 1932 (2014).
29. S. Ou, G. Liu, L. Guo, Z. Zhang, and Q. Zhang, Appl. Opt. **57**, 5068 (2018).
30. T. Jiang, Y. Cui, P. Lu, C. Li, A. Wang, and Z. Zhang, IEEE Photon. Technol. Lett. **28**, 1786 (2016).
31. W. Hansel, H. Hoogland, M. Giunta, S. Schmid, T. Steinmetz, R. Doubek, P. Mayer, S. Dobner, C. Cleff, M. Fischer, and R. Holzwarth, Appl. Phys. B **123**, 41 (2017).
32. G. Liu, A. Wang, and Z. Zhang, IEEE Photon. Technol. Lett. **29**, 2055 (2017).
33. W. Liu, H. Shi, J. Cui, C. Xie, Y. Song, C. Wang, and M. Hu, Opt. Lett. **43**, 2848 (2018).
34. S. Boscolo, S. Turitsyn, and K. Blow, Opt. Fiber Technol. **14**, 299 (2008).
35. A. Komarov, H. Leblond, and F. Sanchez, Phys. Rev. A **71**, 053809 (2005).
36. G. P. Agrawal, *Nonlinear Fiber Optics*, 5th ed. (Elsevier, 2013).
37. E. M. Dianov, A. Y. Karasik, P. V. Mamyshev, A. M. Prokhorov, V. N. Serkin, M. F. Stelmakh, and A. A. Fomichev, JETP Lett. **41**, 294 (1985).